ACCOUNTS of chemical research

Article

pubs.acs.org/accounts

Highly Confined Water: Two-Dimensional Ice, Amorphous Ice, and Clathrate Hydrates

Wen-Hui Zhao,[†,§] Lu Wang,[†,§] Jaeil Bai,[‡,§] Lan-Feng Yuan,[†] Jinlong Yang,[†] and Xiao Cheng Zeng*[,†,‡]

[†]Hefei National Laboratory for Physical Sciences at Microscale and Collaborative Innovation Center of Chemistry for Energy Materials, Department of Chemical Physics, University of Science and Technology of China, Hefei, Anhui 230026, China

[‡]Department of Chemistry, University of Nebraska—Lincoln, Lincoln, Nebraska 68588, United States

Supporting Information

CONSPECTUS: Understanding phase behavior of highly confined water, ice, amorphous ice, and clathrate hydrates (or gas hydrates), not only enriches our view of phase transitions and structures of quasi-two-dimensional (Q2D) solids not seen in the bulk phases but also has important implications for diverse phenomena at the intersection between physical chemistry, cell biology, chemical engineering, and nanoscience. Relevant examples include, among others, boundary lubrication in nanofluidic and lab-on-a-chip devices, synthesis of antifreeze proteins for ice-growth inhibition, rapid cooling of biological suspensions or quenching emulsified water under high pressure, and storage of H_2 and CO_2 in gas hydrates. Classical molecular simulation (MD) is an indispensable tool to explore states and properties of highly confined water and ice. It also has the advantage of precisely monitoring the time and spatial domains in the sub-picosecond and sub-nanometer scales, which are difficult to control in laboratory experiments, and yet allows relatively long simulation at the 10^2 ns time scale that is impractical with *ab initio* molecular dynamics simulations.

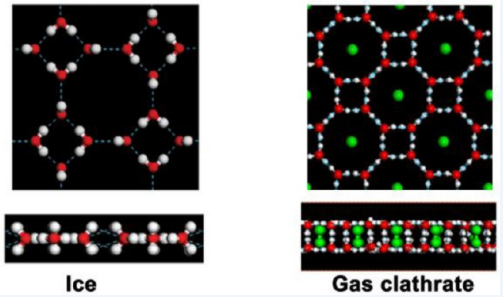

In this Account, we present an overview of our MD simulation studies of the structures and phase behaviors of highly confined water, ice, amorphous ice, and clathrate, in slit graphene nanopores. We survey six crystalline phases of monolayer (ML) ice revealed from MD simulations, including one low-density, one mid-density, and four high-density ML ices. We show additional supporting evidence on the structural stabilities of the four high-density ML ices in the vacuum (without the graphene confinement), for the first time, through quantum density-functional theory optimization of their free-standing structures at zero temperature.

In addition, we summarize various low-density, high-density, and very-high-density Q2D bilayer (BL) ice and amorphous ice structures revealed from MD simulations. These simulations reinforce the notion that the nanoscale confinement not only can disrupt the hydrogen bonding network in bulk water but also can allow satisfaction of the ice rule for low-density and high-density Q2D crystalline structures.

Highly confined water can serve as a generic model system for understanding a variety of Q2D materials science phenomena, for example, liquid−solid, solid−solid, solid−amorphous, and amorphous−amorphous transitions in real time, as well as the Ostwald staging during these transitions. Our simulations also bring new molecular insights into the formation of gas hydrate from a gas and water mixture at low temperature.

1. INTRODUCTION

Bulk water and ice always attract enormous interest due to their relevance to many branches of natural sciences, from biology to chemistry and from earth and planetary science to physics. It is known that bulk ice has 15 crystalline polymorphs (ice I_h, ice I_c, and ice II−XIV) and at least three amorphous structures (low-density, high-density, and very high-density amorphous, that is, LDA, HDA, and VHDA[1−4]). Among the 15 crystalline polymorphs, the metastable ice I_c is believed to be not truly cubic but composed of randomly stacked cubic and hexagonal layers.[5−7] Furthermore, water and gas together can form ice clathrate hydrates at low temperatures, that is, ice-like crystalline compounds comprised of gas molecules trapped inside hydrogen-bonded water cages.[8] Highly confined environment at the nanoscale can disrupt the hydrogen-bonding network in water and thus multiply the number of possible polymorphs of quasi-two-dimensional (Q2D) ice at low temperatures. It is also known that water molecules next to a solid wall can undergo stratification that extends two to three molecular diameters. Since our report of the first simulation evidence of spontaneous formation of bilayer hexagonal ice in 1997 (bilayer ice I) for water confined in a graphene slit nanopore,[9] numerous quasi-one-dimensional (Q1D) and Q2D ice polymorphs have been revealed from MD simulations, experiments, or both, such as *n*-polygonal (n = 5−9) ice nanotubes inside carbon nanotubes[10−16] and Q2D monolayer,[17−21] bilayer,[22−27] and trilayer[28,29] ice polymorphs within *hydrophobic* slit nanopores. A

Received: April 16, 2014
Published: August 4, 2014

   dx.doi.org/10.1021/ar5001549 | Acc. Chem. Res. 2014, 47, 2505−2513

Table 1. DFT Optimized Geometric Structures (top and side views), Water Models and Long-Ranged Electrostatic Interaction (LR-EI) Treatment in Classical MD Simulations and Ferroelectricity of ML-ices I–VI[a]

Monolayer Ice index	DFT Optimized Structure (O: red ball; H: white ball; C: gray; HB: blue;)	Description of Geometric Structure	Water Model; LR-EI Treatment	Area Density (nm^{-2})	Ferroelectricity
ML-ice I (LD-48MI) (Refs. 20,30)	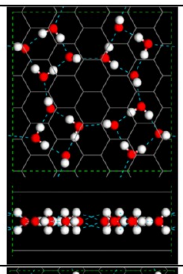	Archimedean $4\cdot8^2$ truncated square tiling	TIP5P; Cut-off or particle-mesh Ewald method (PME)	~9	N
ML-ice II (MD-HMI) (Ref. 30)	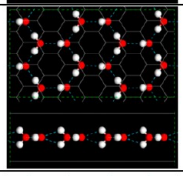	Planar hexagonal morphology with the hexagonal rings elongated along the polarization direction	TIP5P; PME or application of an in-plane electric field	~11	Y
ML-ice III (HD-fRMI) (Ref. 30)	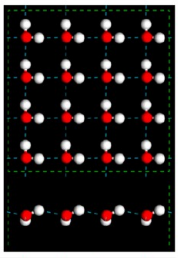	Planar rhombic morphology with the feature of out-of-the-O-plane H atoms	TIP5P; PME or application of an in-plane electric field	~13	Y
ML-ice IV (HD-pRMI) (Refs. 17,30)	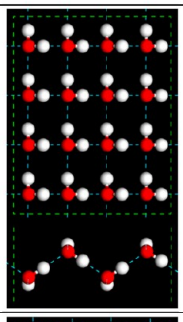	Puckered rhombic morphology	TIP5P; PME or application of an in-plane electric field	~>13.7	Y
ML-ice V (Refs. 18-21)	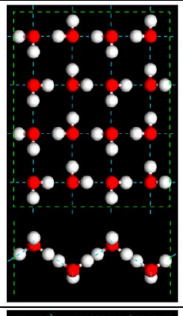	Puckered rhombic morphology without net polarization	TIP4P, TIP3P, SPC, SPCE); Cut-off or PME; --- TIP5P; Cut-off	~>13.7	N
ML-ice VI	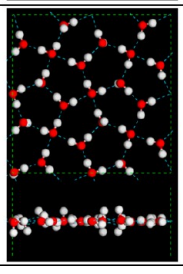	Snub square tiling (irregular pentagons)	TIP5P; PME	~12.5	N

[a]ML-ices III–VI are stable as free-standing ice in vacuum, whereas ML-ices I and II are stable only under confinement of two graphene sheets.

comprehensive phase diagram of Q1D ice phases (ice nanotubes) in carbon nanotubes was presented by Takaiwa et al.,[13] which includes seven single-walled, one double-walled, and one triple-walled ice nanotubes. However, a comprehensive phase

dx.doi.org/10.1021/ar5001549 | Acc. Chem. Res. 2014, 47, 2505–2513

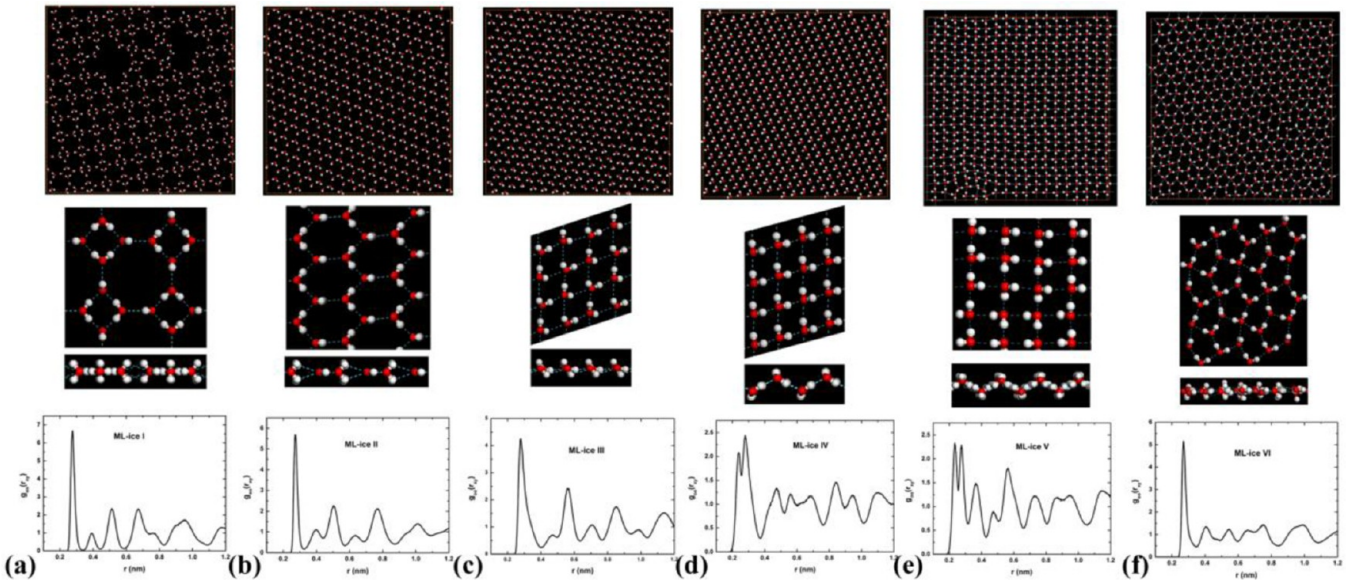

Figure 1. Top view (upper row) and magnified view (middle row) of inherent structures and lateral oxygen−oxygen radial distribution functions ($g_{OO}(r_{xy})$, bottom row) of ML ices formed between two parallel hydrophobic walls: (a) low-density ML-ice I (square-octagonal or $4{\cdot}8^2$ ice); (b) mid-density ML-ice II (hexagonal ice); (c) high-density ML-ice III (flat rhombic ice); (d) high-density ML-ice IV (puckered ferroelectric rhombic ice); (e) high-density ML-ice V (puckered nonferroelectric rhombic ice); (f) high-density ML-ice VI (snub square tiling with irregular pentagons); Parts a−d adapted with permission from ref 30. Copyright 2014 Royal Society of Chemistry.

diagram of Q2D ice polymorphs in graphene slit nanopores is still lacking. In this Account, we summarize recent findings of new Q2D ice polymorphs, amorphous ices, and gas hydrates from MD simulations to obtain a more comprehensive picture about phase behavior of highly confined water, Q2D ice, and gas hydrates. At present, 12 distinctive 2D polymorphous and polyamorphous ice structures are observed from our simulations of water confined between two parallel hydrophobic sheets about 5−10 Å apart. Based on the layers of 2D ices, the twelve 2D ice structures can be classified into three types: (1) for $D < 7$ Å, six distinctive ML ice polymorphs can be easily formed spontaneously; (2) for $7 < D < 9$ Å, spontaneous formation of two BL crystalline ice polymorphs and three BL polyamorphous ice structures is observed; (3) for $D = 10$ Å, a trilayer (TL) ice structure is observed. Additional evidence on structural stabilities of the four high-density ML ices are provided for the first time through quantum density-functional theory (DFT) optimization of their free-standing structures in vacuum at zero temperature.

2. MONOLAYER ICES

Table 1 displays structures of six distinctive ML ice polymorphs observed in our MD simulations of water confined between two parallel hydrophobic walls (either smooth or atomistic graphene walls) about 5−7 Å apart. These six ML ices are the low-density square-octagonal or $4{\cdot}8^2$ monolayer ice (LD-48MI) or ML-ice I,[20,30] the mid-density hexagonal monolayer ice (MD-HMI) or ML-ice II,[30] high-density flat rhombic monolayer ice (HD-fRMI) or ML-ice III,[30] high-density puckered rhombic monolayer ice (HD-pRMI) with ferroelectricity or ML-ice IV,[17,30] high-density puckered rhombic monolayer ice (ML-ice V),[18−21] and high-density irregular pentagonal monolayer ice (ML-ice VI, resembling the snub square tiling). Stability of ML-ices III−VI in vacuum (without the confinement) is also confirmed by DFT optimization (see the Supporting Information).

Spontaneous formation of ML-ice I from 2D water is observed in hydrophobic slits with width 5−6 Å at low lateral pressure and 200 K.[20,30] As shown in Table 1 and Figure 1a, the inherent structure of ML ice I resembles the Archimedean $4{\cdot}8^2$ truncated square tiling. Its area density is lowest among the six ML ices, about 9 nm^{-2}. Thus, far, ML ice I is the only low-density monolayer ice found. All oxygen atoms in ML-ice I are located in the same plane, exhibiting a planar morphology. Every water molecule in ML-ice I has three nearest-neighbor water molecules. Thus, it appears that ML-ice I does not satisfy the ice rule (the ice rule states that every water molecule participates in four hydrogen bonds with nearest-neighbor water molecules). However, every molecule actually acts as either a "double donor to a single acceptor" or a "double acceptor of a single donor", forming totally two weak and two strong hydrogen bonds.[30] The plane of every water molecule is perpendicular to the planes of three nearest-neighbor molecules. Under confinement of two graphene sheets, structural stability of the ML-ice I is confirmed via DFT optimization and vibrational-frequency analysis (see Supporting Information). However, without graphene confinement, the optimized free-standing ML-ice I loses the two-centered hydrogen-bonding feature, thereby not satisfying the ice rule. Note that a previously reported adlayer ice structure on a hydroxylated silica surface exhibits similar structure to the ML-ice I.[31] Owing to the strong interaction between water molecules and the underlying hydrophilic silica surface, the adlayer ice does not satisfy the ice rule.

By compression of ML-ice I in the lateral direction in the MD simulation, middle-density ML-ice II with a hexagonal structure can be obtained. This solid-to-solid transition resembles the bulk ice I_h-to-ice III transition.[32] The planar hexagonal morphology also meets the ice rule like ML-ice I (see Table 1 and Figure 1b). The abrupt change in the area density indicates that the transition from ML-ice I to ML-ice II is a strong first-order polymorphic transition. Moreover, the Ostwald staging phenomenon[33] (i.e., the appearance of an intermediate liquid phase (short-lived) between the solid-to-solid transition) is observed during the 2D solid−solid transition between two ice phases. Despite similarity in the H-bonding pattern, ML-ice II

dx.doi.org/10.1021/ar5001549 | Acc. Chem. Res. 2014, 47, 2505−2513

and ML-ice I still exhibit some qualitative differences in their structural motifs, particularly their intrinsic polarization. In ML-ice I, dipole moments of water molecules offset one another, resulting in zero total dipole. To the contrary, the dipole vectors of all water molecules in ML-ice II are parallel to the longest diagonal of a hexagon. Thus, ML-ice II exhibits significant net polarization. In fact, a strong ferroelectric hysteresis loop can be observed, indicating that the ML-ice II is ferroelectric. Under confinement of the two graphene sheets, structural stability and ferroelectricity of the ML-ice II are also confirmed via DFT optimization (see Supporting Information). Like ML-ice I, when ML-ice II is optimized without the graphene confinement, the free-standing ML-ice II loses the two-centered hydrogen-bonding feature, thereby no longer satisfying the ice rule.

High-density ML-ice III can be obtained through a strong lateral compression of the middle-density ML-ice II. Upon the transition toward ML-ice III, again, an intermediate monolayer liquid is observed. The solid-to-liquid-to-solid phase transitions are akin to the bulk ice I_h-to-liquid water-to-ice III phase transition.[32] ML-ice III is composed of rhombic rings (Table 1 and Figure 1c). Unlike ML-ice I or ML-ice II in which the plane of every water molecule is either parallel or normal to the plane of ice, all planes of H_2O molecules actually tilt with respect to the plane of oxygen. The tilted molecular planes are largely a manifestation of the high-density ice, resulting in a highly frustrated H-bonding network. Still, the flat structure (i.e., all oxygen and hydrogen atoms of water molecules are in the same plane) of rhombic ice can be also attained by using three-site or four-site[21] water models in MD simulations. However, DFT optimization indicates that the flat structure is unstable, largely due to incompatibility with the sp^3 hybridization of oxygen atoms in the 3-site or 4-site water models.[30]

ML-ice IV, first reported by Zangi and Mark,[17] also exhibits rhombic rings. It is formed spontaneously in a slightly wider slit (not sufficiently wide to accommodate two layers of water). Unlike ML-ices I–III, oxygen atoms of ML-ice IV are in alternative ridges with different height in the normal direction (see Table 1 and Figure 1d). So ML-ice IV exhibits a nonplanar "puckered" structure. Analysis of the hydrogen bonding shows that a half number of hydrogen bonds (HBs) along the ridges are frustrated as in the case of ML-ice III, but another half between nearest neighboring ridges are aligned linearly. The ML-ice IV differs from ML-ice III even though both are high-density ice with rhombic rings. A strong hysteresis shown in the potential-energy curves during the expansion/compression of the slit width suggests a strong first-order polymorphic transition from ML-ice III to ML-ice IV. Since both ML-ice III and ML-ice IV exhibit notable net polarizations, both ices are predicted to be ferroelectric.

Like ML-ice IV, ML-ice V (Figure 1e and Table 1) also exhibits puckered rhombic structure, and it was also obtained in our previous MD simulations using a cutoff method (i.e., neglecting long-ranged electrostatic interactions).[18−21] The ML-ice V is *nonpolarized* and hence not ferroelectric, whereas the ferroelectric ML-ice IV is more likely to form if the slab-adapted Ewald sum method is used for treating the long-ranged electrostatic interactions.[34] The ferroelectric ML-ices II and III cannot be observed if the cutoff method is used, indicating the importance of considering long-ranged electrostatic interactions to the formation of ferroelectric ML ices. However, when the ML water is subjected to a strong in-plane electric field, the ML-ices II and III can still arise at low temperature even with use of the cutoff method. Under the same electric field, the nonpolarized ML-ice V can become polarized as well, that is, can transform into ML-ice IV. In some sense, the use of either the Ewald sum method or an in-plane electric field can be viewed as two effective ways to restore underestimated long-ranged electrostatic interactions (like the cutoff potential).

All ML ices I–V structures satisfy the ice rule. However, ML-ice VI, identified as five-membered hydrogen-bonded rings (planar irregular pentagons), appears not to satisfy the ice rule (see Figure 1f and Table 1). ML-ice VI resembles snub square tiling with vertex configuration $3^2{\cdot}4{\cdot}3{\cdot}4$, identical to a layer of the "coffins" bilayer ice reported by Johnston et al.[26] The area density of ML-ice VI is about 12.5 nm^{-2}, slightly lower than those of ML-ices III (~13 nm^{-2}), IV (>13.7 nm^{-2}), and V (>13.7 nm^{-2}), but higher than those of ML-ices I (~9 nm^{-2}) and II (~11 nm^{-2}). Thus, we identify it as a high-density ice.

The first peak in the lateral O–O RDF of the ML-ices I, II, III, and VI is located at ~0.28 nm (Figure 1), a value close to that of the nearest neighbor in bulk water, suggesting that all oxygen atoms of the four ML ices are located in the same plane. On the other hand, the first two peaks in the RDF of ML-ices IV and V are located at ~0.24 and ~0.28 nm, indicating that one type of hydrogen bond is nearly parallel to the confinement walls and another type is not parallel to the walls.

The rich phase behavior of monolayer water and ices can be illustrated by schematic P_L–T phase diagrams displayed in Figure 2 for D = 0.52, 0.557, 0.62, and 0.65 nm. More accurate phase

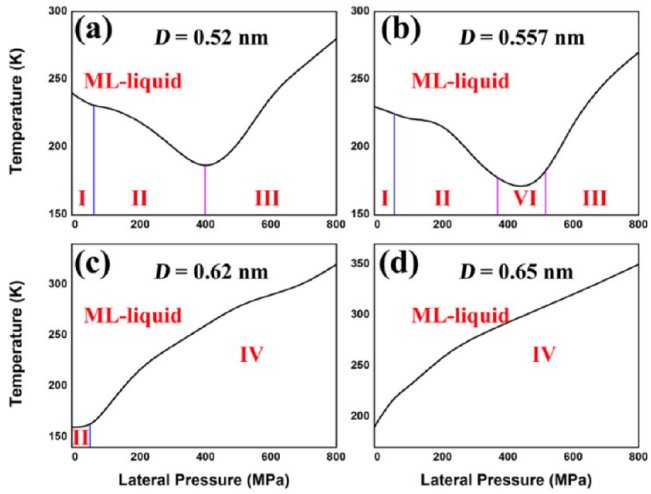

Figure 2. Schematic semiquantitative P_L–T phase diagrams for ML ices (with PME treatment in MD simulation).

boundaries can be determined via the multibaric–multithermal ensemble approach that involves an anisotropic pressure control.[21] As shown in Figure 2a, for D = 0.52 nm, ML-ices I, II, and III are observed. With increasing the lateral pressure, melting temperatures of ML-ices I and II decrease, while that of ML-ice III increases. The negative slope of liquidus lines of ML-ices I and II resembles that of bulk ice I_h.[32] For D = 0.557 nm, besides the ML-ices I, II, and III, ML-ice VI can be formed spontaneously at ~170 K and 400–500 MPa (Figure 2b). Again, increasing the lateral pressure will lower the melting temperatures of ML-ices I and II but raise that of ML-ice III. For D = 0.62 nm, ML-ices I, III, and VI are absent, while ML-ice II remains at low pressure and ~160 K (Figure 2c). Note that ML-ice I is a metastable phase at negative pressure, and it can transform into ML-ice II through repeated cycles of cooling and heating. Beyond 50 MPa (lateral pressure), ML-ice IV is formed,

dx.doi.org/10.1021/ar5001549 | Acc. Chem. Res. 2014, 47, 2505–2513

and its melting temperature increases with the lateral pressure. For D = 0.65 nm, only ML-ice IV can be formed (Figure 2d).

We note another hexagonal ML ice that can be formed between two finite-sized SiO_2 slabs.[22] This ML ice exhibits an all-atom flat structure and is nonpolarized. Because each water molecule is involved in only three in-plane hydrogen bonds, this ML ice cannot meet the ice rule. Besides the six ML ice polymorphs illustrated in Table 1, structural properties of ML adlayer ice confined between a hydrophobic surface (graphene) and a hydrophilic surface (mica) have been recently studied by Heath and co-workers[35] using atomic-force microscopy and by us using Born−Oppenheimer MD simulation.[36] This ML adlayer ice is not free-standing due to the strong interaction between water molecules and the mica surface. Several other ML adlayer ices have been observed in simulations[31,37] or experiments.[38−40] The "probably ferroelectric" ML ice, observed by Spagnoli et al.,[39] can be formed on an exposed mica surface, and its structure resembles that of ML-ice IV.[30]

The low-density ML ice I can be also viewed as a guest-free ML ice clathrate because it contains relatively large octagon "cages" that are large enough to accommodate a gas atom. Indeed, spontaneous formation of ML argon ice clathrate (or ML argon hydrate) is observed in our simulations.[20] Here the water framework underlying the ML argon hydrate is exactly the same as ML-ice I, where each octagon ring can accommodate a single Ar atom (Figure 3).

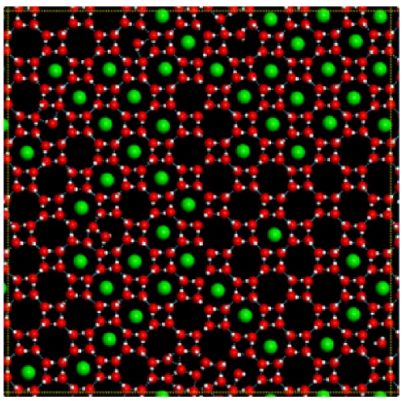

Figure 3. Inherent structure of ML argon hydrate formed between two hydrophobic planar walls. Red, white, and green spheres represent oxygen, hydrogen, and argon, respectively, and blue lines represent hydrogen bonds. Adapted with permission from ref 20. Copyright 2010 National Academy of Sciences.

To date, at least six crystalline polymorphs of ML ice are observed in MD simulations. However, ML amorphous ice has not been observed directly from MD simulation of monolayer water confined between two parallel graphene sheets. Remarkably, Davies and co-workers[41] recently detected formation of monolayers of a polypentagonal water network within the hydrophobic core of an antifreeze protein called Maxi (in nature, such an antifreeze protein can protect the winter flounder from subzero temperature conditions). Davies and workers found that the polypentagonal water network is amorphous, consisting of about 400 waters. This ML amorphous ice is largely due to the *molecularly rough* inner-surface architecture of the Maxi protein, which is unlike the smooth surface of a graphene sheet. The molecularly rough inner-surface architecture induces five-membered water rings to form cages on individual residues (semiclathrate structure). Hence, the ML amorphous ice is nonplanar. The experimental evidence of the existence of ML amorphous ice suggests that ML amorphous ice may be a metastable phase for monolayer water confined between two parallel graphene sheets. However, because the tendency toward the formation of ML ice is very high (due to low free-energy barriers separating ML water and ML ices), the formation of ML amorphous ice is always preempted by ML ices.

3. BILAYER ICE AND AMORPHOUS ICE

As pointed out above, thus far, ML amorphous ice has not been achieved directly from MD simulation of monolayer water confined between two parallel graphene sheets. In such a molecularly smooth confinement, it appears that the thinnest and most stable Q2D amorphous ice is bilayer (BL) amorphous ice. In our previous MD simulations, we observed spontaneous formation of two BL crystalline ice polymorphs and three BL polyamorphous ice structures for water confined between two parallel hydrophobic sheets about 7−9 Å apart. These BL polymorphous and polyamorphous ice structures are identified as BL hexagonal ice (BL-ice I, with area density ∼21 nm^{-2}),[9] BL very-high-density crystalline ice (BL-VHDI, ∼26.5 nm^{-2}),[27] BL-amorphous ice (BL-A, ∼20 nm^{-2}),[23] BL very-high-density amorphous ice I (BL-$VHDA_1$, ∼23.5 nm^{-2}),[25,27] and BL very-high-density amorphous ice II (BL-$VHDA_2$, ∼25.8 nm^{-2}).[27]

BL-amorphous ice (BL-A) exhibits polygonal structure with predominantly hexagonal, heptagonal, and pentagonal rings (Figure 4a). In BL-A, the two monolayers are in registry. BL-A can be easily formed from BL water in the temperature range of 200−270 K.[23] Depending on the polygonal ring distribution, the width (D) of the nanoslit, and the magnitude of the lateral pressure, the area density of the BL-A can be either lower or higher than that of the initial BL liquid. BL-A is more likely a metastable phase since BL-hexagonal ice (BL-ice I) can be formed by annealing the BL-A through repeated cycles of cooling and heating.[42] Both BL ice-I and BL-A satisfy the ice rule.

BL-$VHDA_2$ is mostly composed of antistacked parallelograms (Figure 4c), and it can be directly produced from the hexagonal BL-ice I at 250 K by increasing the lateral pressure stepwise from 0 to 2.9 GPa. In turn, if the $VHDA_2$ is decompressed stepwise from 3 GPa at 250 K, it turns into the BL-A at 1 GPa. Moreover, if the BL-$VHDA_2$ is decompressed instantly from 3 to 1.5 GPa at 250 K, it turns into BL-$VHDA_1$ spontaneously. BL-$VHDA_1$, exhibiting mostly pentagons (Figure 4b), was first observed by Han, Stanley, and co-workers in their MD simulations.[25] BL-$VHDA_1$ can be also obtained by cooling the BL liquid under 2.0 GPa. At 0 K, BL-$VHDA_1$ is energetically more favorable than BL-$VHDA_2$ because the potential energy of BL-$VHDA_1$ is lower than that of BL-$VHDA_2$. Moreover, at 1.5 GPa and 250 K, the spontaneous transformation of $VHDA_2$-to-$VHDA_1$ can occur. The abrupt changes in the area density and potential energy during the compression or decompression suggest that the BL-ice I-to-$VHDA_2$, $VHDA_2$-to-BL-A, and $VHDA_2$-to-$VHDA_1$ transitions are all strong first-order polyamorphous transitions. Neither BL-$VHDA_1$ nor BL-$VHDA_2$ satisfies the ice rule because of the very-high-density packing. The polymorphic transition of BL-ice I to BL-VHDA is akin to the pressure induced bulk ice I_h to HDA transition.[1] Contrary to the BL-A ↔ $VHDA_2$ transition, which is strongly first order, the bulk LDA ↔ HDA transition has been viewed as "apparently first-order",[1] whereas the bulk HDA ↔ VHDA transition may be viewed either as a first-order or kinetic densification.[3] The true nature of the first-order transition between bulk LDA, HDA, and VHDA is still inconclusive.[4]

dx.doi.org/10.1021/ar5001549 | *Acc. Chem. Res.* 2014, 47, 2505−2513

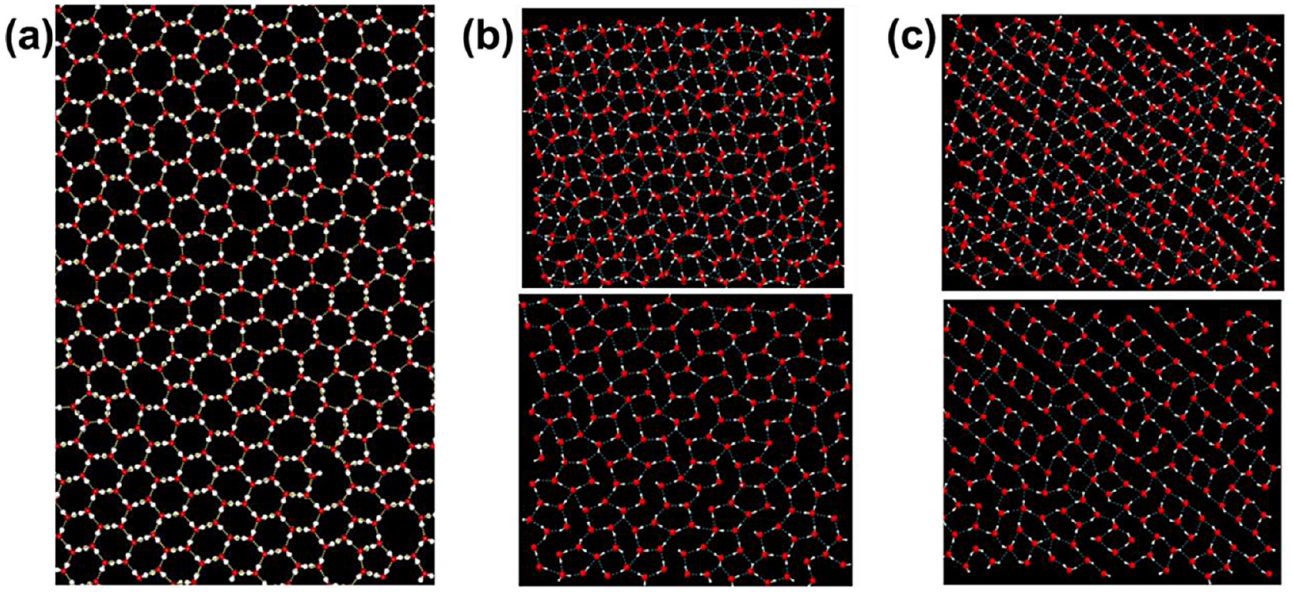

Figure 4. Inherent structures of bilayer amorphous (BL-A) and very-high-density amorphous (BL-VHDA) ices: (a) top view of BL-A; (b) top view of BL-VHDA$_1$ (mostly composed of pentagons) (upper panel) and top view of bottom monolayer of BL-VHDA$_1$ (lower panel); (c) top view of BL-VHDA$_2$ (mostly composed of antistacked parallelograms) (upper panel) and top view of bottom monolayer of VHDA$_2$ (lower panel). Panel a was adapted with permission from ref 23. Copyright 2000 Macmillan Publishers Ltd.: Nature. Panels b and c were adapted with permission from ref 27. Copyright 2012 National Academy of Sciences.

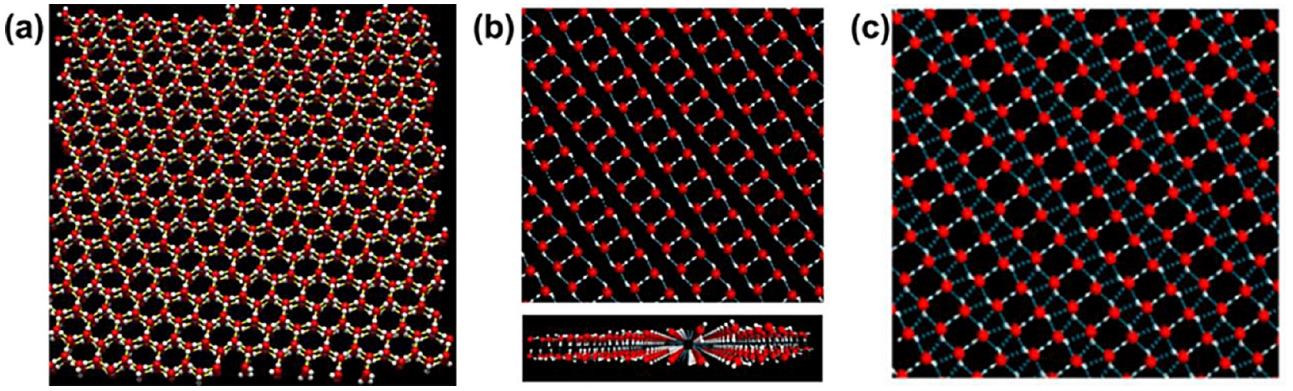

Figure 5. Inherent structure of bilayer ices formed between two parallel hydrophobic walls: (a) BL-ice I; (b) top (upper panel) and side (lower panel) views of BL-VHDI without displaying the "inter-tube" hydrogen bonds; (c) top view of BL-VHDI. Panel a was adapted with permission from ref 9. Copyright 1997 The American Physical Society. Panels b and c were adapted with permission from ref 27. Copyright 2012 National Academy of Sciences.

BL-ice I is composed of two hexagonal monolayers of water and both monolayers are in registry (Figure 5a).[9] The BL-ice I has been successfully grown in the laboratory through vapor deposition on graphene/Pt(111) substrate.[43] To our knowledge, BL-ice I is the first free-standing Q2D ice observed in nature. Using a more simplified mW model water, Kastelowitz et al.[44] found another marginally stable BL hexagonal ice but with puckered hexagonal rings, namely, BL puckered hexagonal ice. This ice forms in a wider pore (D = 10.5 Å) and at 1 atm lateral pressure. The two monolayers of the BL puckered ice seem slightly out of registry. Besides the BL-ice I, a number of other mid-density BL ice phases have been reported in the literature, such as BL-Cairo pentagonal ice,[26] BL-mixed pentagon hexagonal ice,[26] BL-quasicrystal ice with 12-fold symmetry,[26] and BL-rhombic ice,[24] indicating much richer BL ice polymorphs compared with ML ice polymorphs.

Lastly, BL-VHDI can be obtained directly from the BL-ice I through an instant lateral compression from 0 to 6 GPa at 250 K. The structure of the BL-VHDI can be viewed as an array of square ice nanotubes (Figure 5b). Within each square "ice nanotube", the ice rule is satisfied, as is the case for the square ice nanotube reported in CNTs.[10] However, the BL-VHDI itself does not satisfy the ice rule because of the existence of the weaker intertube hydrogen bonds between any two neighbor square ice nanotubes (Figure 5c).

4. BILAYER CLATHRATE

Unlike for ML-ice I, low-density BL ice with Archimedean 4·8^2 (square-octagon) pattern cannot be formed spontaneously from BL water at low temperature. In other words, the guest-free BL clathrate is unlikely to be stable. With guest molecules trapped in the octagonal BL rings, BL crystalline and amorphous clathrates have been observed in our MD simulations of BL mixtures of water and gas molecules confined between two parallel hydrophobic walls.[27] The guest molecules examined thus far include methane and ethane (see Figure 6). In the BL gas

dx.doi.org/10.1021/ar5001549 | Acc. Chem. Res. 2014, 47, 2505−2513

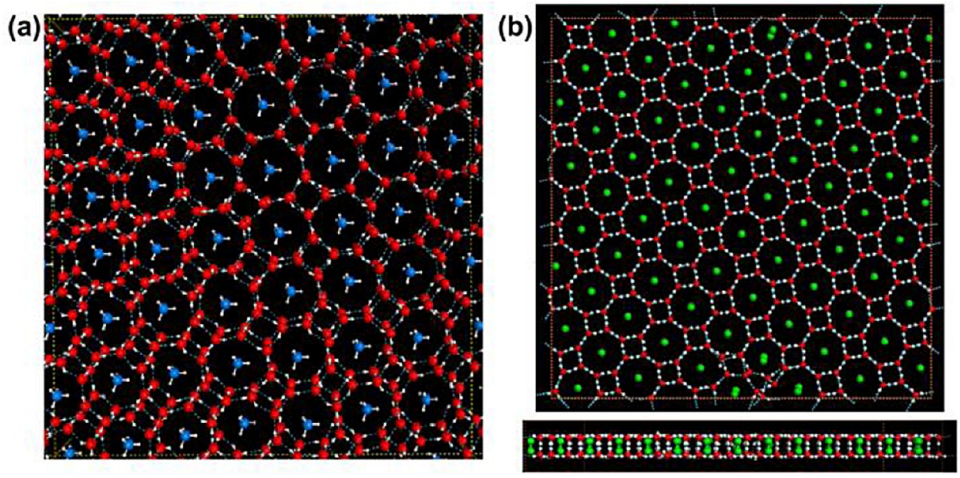

Figure 6. Inherent structure of bilayer gas hydrates with (a) methane (blue) or (b) ethane (green) as guest molecules. Panel a was adapted with permission from ref 27. Copyright 2012 National Academy of Sciences.

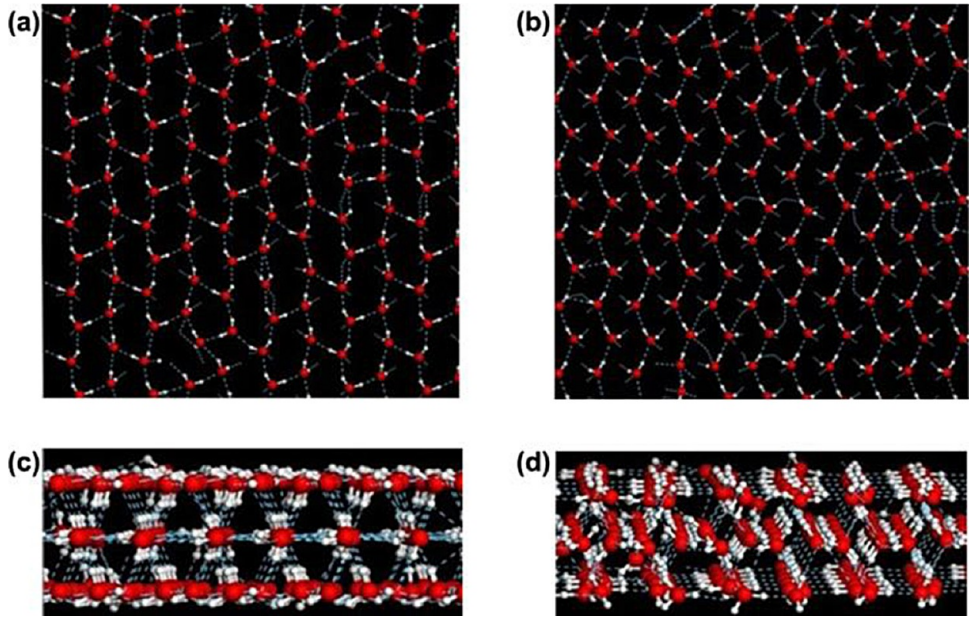

Figure 7. Inherent structure of a trilayer distorted-rectangle-rhombic ice: top views of the (a) top and (b) middle layers, respectively; (c, d) side views in two lateral directions. Adapted with permission from ref 29. Copyright 2014 Chinese Physical Society.

hydrates, each octagonal ring contains only one guest molecule. The longer molecular axis of the ethane molecule is always perpendicular to the plane of the ice clathrate. The tetragonal rings connect the octagonal rings together.

Typically, when the BL gas/water mixtures are annealed directly in the slit pores, long-range crystalline order is difficult to achieve. In most cases, crystalline hydrates tend to nucleate via amorphous intermediates, in analogy to the formation of the BL-ice I via the metastable BL-A.[27,42] In the BL amorphous gas hydrates, the BL-polygonal defects (BL-pentagonal rings in particular) tend to form between BL-octagonal rings. The BL-pentagonal rings can maintain their structural integrity along with the BL-octagonal rings to hinder the formation of BL-crystalline hydrates. Moreover, because the solubility of guest gas molecules in liquid water is very low, gas bubbles can be formed at the early stage. Some dense bubbles may be trapped in the clathrate to obstruct the formation of crystalline clathrate. So phase-separation-like behavior may occur before and even during the formation of various types of clathrate hydrates not only in nanoslit but also in bulk. Typically, to remove the undesirable BL-pentagonal rings or dense bubbles, one can use multistep MD simulation procedures, including cyclic heating/annealing, stepwise compression, and long-time incubation.

5. TRILAYER ICES

Few MD simulation studies of trilayer ice polymorphs or amorphous ice have been reported in the literature. Our recent simulation of water confined between two smooth hydrophobic walls with D = 1.0 nm results in a trilayer (TL) ice structure (Figure 7) at 290 K and 1 GPa lateral pressure.[29] Here, the oxygen atoms form three parallel planar layers; the water molecules in the outmost two layers form distorted rectangles, and those in the middle layer form rhombic rings. We thus identify the Q2D ice as TL distorted-rectangle-rhombic ice whose area density is ∼35 nm^{-2}. This high-density TL ice satisfies the ice rule. For each molecule in the outmost two layers,

dx.doi.org/10.1021/ar5001549 | Acc. Chem. Res. 2014, 47, 2505−2513

three of its four HBs are in one layer, while the fourth HB connects with the middle layer. For each molecule in the middle layer, only two out of the four HBs are located in the same layer, while the other two HBs connect with two outmost layers.

Four other TL ice structures reported in the literature include the trilayer heterogeneous fluid revealed by Giovambattista et al.[28] in their MD simulation of water confined to two silica-based hydrophobic surfaces with D = 0.8 nm at a mass density >1.05 g/cm^3. The trilayer heterogeneous fluid is characterized by a middle liquid layer and two outer crystal-like layers. The second TL ice reported by Kumar et al.[18] is formed in the slit pore with D = 1.1 nm at the density 1.32 g/cm^3. Here, the two outer layers are flat while the middle layer is puckered. The third and the fourth TL ices, found by Kastelowitz et al.,[44] are planar (for D = 1.1−1.15 nm) and puckered (for D = 1.2−1.4 nm), respectively. In the planar TL ice, every water molecule has four HB nearest-neighbors. The puckered TL ice can be viewed as a slab of ice I_h, where each water molecule in the two outer layers forms only three HBs.

6. SUMMARY AND FUTURE OUTLOOK

We have surveyed various monolayer, bilayer, and trilayer polymorphous and polyamorphous ice structures reported since 1997[9] and monolayer and bilayer clathrates (or gas hydrates) reported since 2010.[20] The rich polymorphs of Q2D ices and clathrates call for future experiments. A future effort in Q2D ices will be polymorphous and polyamorphous structures of four-layer or higher multilayer ices and their phase behavior, phase diagrams, and structural relations with thin films of bulk ice. Another hot topic would be water structures within the hydrophobic core of various antifreeze proteins[41] and phase behavior of highly confined water in more realistic nanoslits with rough surfaces. These studies would have important implications to the design of new artificial surfaces to mimic antifreeze proteins for ice-growth inhibition and cryopreservation.

■ ASSOCIATED CONTENT

Supporting Information

Results of density-functional optimization of the six ML ice structures in vacuum. This material is available free of charge via the Internet at http://pubs.acs.org.

■ AUTHOR INFORMATION

Corresponding Author

*E-mail: xzeng1@unl.edu.

Author Contributions

§W.-H.Z., L.W., and J.B. contributed equally to this work.

Funding

This work is supported by MOST (Grant 2011CB921400), by NSFC (Grants 91021004, 20933006, 21121003, and 2123307), by CAS (Grant XDB01020300), and by Fundamental Research Funds for the Central Universities (Grant WK2060030012). X.C.Z. is supported by grants from the NSF (Grant CHE-1306326) and USTC for Qianren-B summer research. W.-H.Z. and X.C.Z. are also supported by a grant from Bureau of Science & Technology of Anhui Province.

Notes

The authors declare no competing financial interest.

Biographies

Wen-Hui Zhao was awarded his Ph.D. from University of Science and Technology of China (USTC), China, in 2012. He currently works as a postdoctoral researcher at USTC (supervised by Zeng). He uses theory and computer simulations to study the liquids and confined fluids, water (ice) and clathrate.

Lu Wang was awarded his Ph.D. from Peking University, China, in 2008. After postdoctoral research at University of Nebraska at Omaha, he is now an associate professor in USTC. He focuses on density functional calculations of low-dimensional nanomaterials.

Jaei Bai was awarded his Ph.D. from University of Nebraska—Lincoln (UNL) in 2004. After postdoctoral research at UNL, he currently works as a research assistant professor at UNL. His research interests include computer simulation of phase transitions of highly confined water, ice, ice clathrates, and silicon nanostructures.

Lan-Feng Yuan received his Ph.D. in chemistry from USTC, China, in 2001. After postdoctoral research at Cornell University and Princeton University, he currently works as an associate professor in USTC. His research area is theoretical and computational chemistry, including molecular orbital theory, first-principles investigations of clusters and extended systems, and molecular dynamics simulations for confined systems such as water.

Jinlong Yang is currently a Changjiang professor of chemistry, executive dean of School of Chemistry and Materials Science in USTC. He received his Ph.D. degree in condensed matter physics from USTC in 1991. He is a fellow of the American Physics Society, a recipient of the young chemist award from Chinese Chemical Society, and a recipient of a national award (class two) for natural science. His research focuses on developing first-principles methods and computational study of clusters, nanostructures, solid materials, and surfaces.

Xiao Cheng Zeng is the Ameritas Distinguished University Professor of Chemistry at UNL and also a 1000 Talents Program B (Summer Research) Professor at USTC. He received his B.S. degree from Peking University in 1984 and Ph.D. from The Ohio State University in 1989. He did his postdoctoral work at the University of Chicago and UCLA. Zeng is a fellow of the American Association for the Advancement of Science, the American Physical Society, and the Royal Society of Chemistry. He has mentored 22 graduate students and 25 postdoctoral fellows. His research interests include phase behavior of confined water and ice, superhydrophobicity and wetting, structural evolutions of gold and silicon clusters, electronic properties of nanostructures, and nanocatalysis.

■ REFERENCES

(1) Mishima, O.; Calvert, L. D.; Whalley, E. An apparently first-order transition between two amorphous phases of ice induced by pressure. *Nature* **1985**, *314*, 76−78.

(2) Loerting, T.; Salzmann, C.; Kohl, I.; Mayer, E.; Hallbrucker, A. A second distinct structural "state" of high-density amorphous ice at 77 K and 1 bar. *Phys. Chem. Chem. Phys.* **2001**, *3*, 5355−5357.

(3) Debenedetti, P. G.; Stanley, H. E. Supercooled and glassy water. *Phys. Today* **2003**, *56*, 40−46.

(4) Loerting, T.; Schustereder, W.; Winkel, K.; Salzmann, C. G.; Kohl, I.; Mayer, E. Amorphous ice: Stepwise formation of very-high-density amorphous ice from low-density amorphous ice at 125 K. *Phys. Rev. Lett.* **2006**, *96*, No. 025702.

(5) Moore, E. B.; Molinero, V. Is it cubic? Ice crystallization from deeply supercooled water. *Phys. Chem. Chem. Phys.* **2011**, *13*, 20008−20016.

(6) Malkin, T. L.; Murray, B. J.; Brukhno, A. V.; Anwar, J.; Salzmann, C. G. Structure of ice crystallized from supercooled water. *Proc. Natl. Acad. Sci. U.S.A.* **2012**, *109*, 1041−1045.

(7) Kuhs, W. F.; Sippel, C.; Falenty, A.; Hansen, T. C. Extent and relevance of stacking disorder in "ice I_c". *Proc. Natl. Acad. Sci. U.S.A.* **2012**, *109*, 21259−21264.
(8) Sloan, E. D., Jr. Fundamental principles and application of natural gas hydrates. *Nature* **2003**, *426*, 353−359.
(9) Koga, K.; Zeng, X. C.; Tanaka, H. Freezing of confined water: A bilayer ice phase in hydrophobic nanopores. *Phys. Rev. Lett.* **1997**, *79*, 5262−6265.
(10) Koga, K.; Gao, G. T.; Tanaka, H.; Zeng, X. C. Formation of ordered ice nanotubes inside carbon nanotubes. *Nature* **2001**, *412*, 802−805.
(11) Mashl, R. J.; Joseph, S.; Aluru, N. R.; Jakobsson, E. Anomalously immobilized water: A new water phase induced by confinement in nanotubes. *Nano Lett.* **2003**, *3*, 589−592.
(12) Bai, J.; Wang, J.; Zeng, X. C. Multiwalled ice helixes and ice nanotubes. *Proc. Natl. Acad. Sci. U.S.A.* **2006**, *103*, 19664−19667.
(13) Takaiwa, D.; Hatano, I.; Koga, K.; Tanaka, H. Phase diagram of water in carbon nanotubes. *Proc. Natl. Acad. Sci. U.S.A.* **2008**, *105*, 39−43.
(14) Maniwa, Y.; Kataura, H.; Abe, M.; Udaka, A.; Suzuki, S.; Achiba, Y.; Kira, H.; Matsuda, K.; Kadowaki, H.; Okabe, Y. Ordered water inside carbon nanotubes: Formation of pentagonal to octagonal ice-nanotubes. *Chem. Phys. Lett.* **2005**, *401*, 534−538.
(15) Kolesnikov, A. I.; Zanotti, J.-M.; Loong, C. K.; Thyagarajan, P.; Morsvsky, A. P.; Loutfy, R. O.; Burnham, C. J. Anomalously soft dynamics of water in a nanotube: A revelation of nanoscale confinement. *Phys. Rev. Lett.* **2004**, *93*, No. 035503.
(16) Byl, O.; Liu, J. C.; Wang, Y.; Yim, W. L.; Johnson, J. K.; Yates, J. T. Unusual hydrogen bonding in water-filled carbon nanotubes. *J. Am. Chem. Soc.* **2006**, *128*, 12090−12097.
(17) Zangi, R.; Mark, A. E. Monolayer ice. *Phys. Rev. Lett.* **2003**, *91*, No. 025502.
(18) Kumar, P.; Buldyrev, S. V.; Starr, F. W.; Giovambattista, N.; Stanley, H. E. Thermodynamics, structure, and dynamics of water confined between hydrophobic plates. *Phys. Rev. E* **2005**, *72*, No. 051503.
(19) Koga, K.; Tanaka, H. Phase diagram of water between hydrophobic surfaces. *J. Chem. Phys.* **2005**, *122*, No. 104711.
(20) Bai, J.; Angell, C. A.; Zeng, X. C. Guest-free monolayer clathrate and its coexistence with two-dimensional high-density ice. *Proc. Natl. Acad. Sci. U.S.A.* **2010**, *107*, 5718−5722.
(21) Kaneko, T.; Bai, J.; Yasuoka, K.; Mitsutake, A.; Zeng, X. C. New computational approach to determine liquid-solid phase equilibria of water confined to slit nanopores. *J. Chem. Theory Comput.* **2013**, *9*, 3299−3310.
(22) Ferguson, A. L.; Giovambattista, N.; Rossky, P. J.; Panagiotopoulos, A. Z.; Debenedetti, P. G. A computational investigation of the phase behavior and capillary sublimation of water confined between nanoscale hydrophobic plates. *J. Chem. Phys.* **2012**, *137*, No. 144501.
(23) Koga, K.; Tanaka, H.; Zeng, X. C. First-order transition in confined water between high-density liquid and low-density amorphous phases. *Nature* **2000**, *408*, 564−567.
(24) Zangi, R.; Mark, A. E. Bilayer ice and alternate liquid phases of confined water. *J. Chem. Phys.* **2003**, *119*, 1694−1700.
(25) Han, S.; Choi, M. Y.; Kumar, P.; Stanley, H. E. Phase transitions in confined water nanofilms. *Nat. Phys.* **2010**, *6*, 685−689.
(26) Johnston, J. C.; Kastelowitz, N.; Molinero, V. Liquid to quasicrystal transition in bilayer water. *J. Chem. Phys.* **2010**, *133*, No. 154516.
(27) Bai, J.; Zeng, X. C. Polymorphism and polyamorphism in bilayer water confined to slit nanopore under high pressure. *Proc. Natl. Acad. Sci. U.S.A.* **2012**, *109*, 21240−21245.
(28) Giovambattista, N.; Rossky, P. J.; Debenedetti, P. G. Phase transitions induced by nanoconfinement in liquid water. *Phys. Rev. Lett.* **2009**, *102*, No. 050603.
(29) Jia, M.; Zhao, W.-H.; Yuan, L.-F. New hexagonal-rhombic trilayer ice structure confined between hydrophobic plates. *Chin. J. Chem. Phys.* **2014**, *27*, 15−19.
(30) Zhao, W.-H.; Bai, J.; Yuan, L.-F.; Yang, J.; Zeng, X. C. Ferroelectric hexagonal and rhombic monolayer ices. *Chem. Sci.* **2014**, *5*, 1757−1764.
(31) Yang, J.; Meng, S.; Xu, L. F.; Wang, E. G. Ice tessellation on a hydroxylated silica surface. *Phys. Rev. Lett.* **2004**, *92*, No. 146102.
(32) Petrenko, V. F.; Whitworth, R. W. *Physics of Ice*; Oxford University Press: New York, 1999.
(33) Ostwald, W. Z. Studien über die Bildung und Umwandlung fester Körper. *Z. Phys. Chem.* **1897**, *22*, 289−330.
(34) Yeh, I. C.; Berkowitz, M. L. Ewald summation for systems with slab geometry. *J. Chem. Phys.* **1999**, *111*, 3155−3162.
(35) Xu, K.; Cao, P.; Heath, J. R. Graphene visualizes the first water adlayers on mica at ambient conditions. *Science* **2010**, *329*, 1188−1191.
(36) Li, H.; Zeng, X. C. Two dimensional epitaxial water adlayer on mica with graphene coating: An ab initio molecular dynamics study. *J. Chem. Theory Comput.* **2012**, *8*, 3034−3043.
(37) Odelius, M.; Bernasconi, M.; Parrinello, M. Two dimensional ice adsorbed on mica surface. *Phys. Rev. Lett.* **1997**, *78*, 2855−2858.
(38) Janiak, C.; Scharmann, T. G. Two-dimensional water and ice layers: Neutron diffraction studies at 278, 263, and 20 K. *J. Am. Chem. Soc.* **2002**, *124*, 14010−14011.
(39) Spagnoli, C.; Loos, K.; Ulman, A.; Cowman, M. K. Imaging structured water and bound polysaccharide on mica surface at ambient temperature. *J. Am. Chem. Soc.* **2003**, *125*, 7124−7128.
(40) Aarts, I. M. P.; Pipino, A. C. R.; Hoefnagels, J. P. M.; Kessels, W. M. M.; van de Sanden, M. C. M. Quasi-ice monolayer on atomically smooth amorphous SiO_2 at room temperature observed with a high-finesse optical resonator. *Phys. Rev. Lett.* **2005**, *95*, No. 166104.
(41) Sun, T.; Lin, F.-H.; Camphell, R. L.; Allingham, J. S.; Davies, P. L. An antifreeze protein folds with an interior network of more than 400 semi-clathrate waters. *Science* **2014**, *343*, 795−798.
(42) Bai, J.; Zeng, X. C.; Koga, K.; Tanaka, H. Formation of quasi-two-dimensional bilayer ice in hydrophobic slit: A possible candidate for ice XIII? *Mol. Simul.* **2003**, *29*, 619−626.
(43) Kimmel, G. A.; Matthiesen, J.; Baer, M.; Mundy, C. J.; Petrik, N. G.; Smith, R. S.; Dohnalek, Z.; Kay, B. D. No confinement needed: Observation of a metastable hydrophobic wetting two-layer ice on graphene. *J. Am. Chem. Soc.* **2009**, *131*, 12838−12844.
(44) Kastelowitz, N.; Johnston, J. C.; Molinero, V. The anomalously high melting temperature of bilayer ice. *J. Chem. Phys.* **2010**, *132*, No. 124511.